Supplementary information for Demonstrating quantum speed-up in a superconducting two-qubit processor

A. Dewes[1], R. Lauro[1], F.R. Ong[1], V. Schmitt[1], P. Milman[2], P. Bertet[1], D. Vion[1], and D. Esteve[1]

October 18, 2011

[1]Service de Physique de l'Etat Condensé/IRAMIS/DSM (CNRS URA 2464), CEA Saclay, F-91191 Gif-sur-Yvette, France

[2]Laboratoire Matériaux et Phénomènes Quantiques, Université Paris Diderot, Bâtiment Condorcet, 10, rue Alice Domon et Léonie Duquet, F75205 Paris, France

S1. Sample preparation

The sample is fabricated on a silicon chip oxidized over 50 nm. A 150 nm thick niobium layer is first deposited by magnetron sputtering and then dry-etched in a SF_6 plasma to pattern the readout resonators, the current lines for frequency tuning, and their ports. Finally, the transmon qubit, the coupling capacitance and the Josephson junctions of the resonators are fabricated by double-angle evaporation of aluminum through a shadow mask patterned by e-beam lithography. The first layer of aluminum is oxidized in a $Ar-O_2$ mixture to form the oxide barrier of the junctions. The chip is glued with wax on a printed circuit board (PCB) and wire bonded to it. The PCB is then screwed in a copper box anchored to the cold plate of a dilution refrigerator.

S2. Sample parameters

The sample is first characterized by spectroscopy (see Fig. 1.b of main text). The incident power used is high enough to observe the resonator frequency ν_{R}, the qubit line ν_{01}, and the two-photon transition at frequency $\nu_{02}/2$ between the ground and second excited states of each transmon (data not shown). A fit of the transmon model to the data yields the sample parameters $E_{\mathrm{J}}^{\mathrm{I}}/h = 36.2\,\mathrm{GHz}$, $E_{\mathrm{C}}^{\mathrm{I}}/h = 0.98\,\mathrm{GHz}$, $d_I = 0.2$, $E_{\mathrm{J}}^{\mathrm{II}}/h = 43.1\,\mathrm{GHz}$, $E_{\mathrm{C}}^{\mathrm{II}}/h = 0.87\,\mathrm{GHz}$, $d_{\mathrm{II}} = 0.35$, $\nu_{\mathrm{R}}^{\mathrm{I}} = 6.84\,\mathrm{GHz}$, and $\nu_{\mathrm{R}}^{\mathrm{II}} = 6.70\,\mathrm{GHz}$. The qubit-readout anticrossing at $\nu = \nu_{\mathrm{R}}$ yields the qubit-readout couplings $g_0^{\mathrm{I}} \simeq g_0^{\mathrm{II}} \simeq (2\pi)\,50\,\mathrm{MHz}$. Independent measurements of the resonator dynamics (data not shown) yield quality factors $Q_{\mathrm{I}} =$

$Q_{\rm II} = 730$ and Kerr non linearities [13,[1]] $K_{\rm I}/\nu_{\rm R}^{\rm I} \simeq K_{\rm II}/\nu_{\rm R}^{II} \simeq -2.3\pm0.5\times10^{-5}$.

S3. Experimental setup

- Qubit resonant microwave pulses: The qubit drive pulses are generated by two phase-locked microwave generators feeding a pair of I/Q-mixers. The IF inputs are provided by a 4-Channel1 GS/s arbitrary waveform generator (AWG Tektronix AWG5014). Single-sideband mixing in the frequency range of 50-300 MHz is used to generate multi-tone drive pulses and to obtain a high ON/OFF ratio ($>$ 50 dB). Phase and amplitude errors are corrected by applying suitable sideband and carrier frequency dependent corrections to the amplitude and offset of the IF signals.

- Qubit frequency control: Flux control pulses are generated by a second AWG and sent to the chip through a transmission line equipped with 40 dB total attenuation and a pair of 1 GHz dissipative low-pass filters at 4 K. The input signal of each flux line is returned to room temperature through an identical transmission line and measured, which allows to compensate the non-ideal frequency response of the line.

- Readout pulses: The driving pulses for the Josephson bifurcation amplifier (JBA) readouts are generated by mixing the continuous signals of a pair of microwave generators with IF pulses provided by a 1 GS/s arbitrary waveform generator (AWG Tektronix AWG5014). Each readout pulse consists of a measurement part with a rise time of 30 ns and a hold time of 100 ns, followed by a 2 μs long latching part at 90 % of the pulse height.

- Drive and measurement lines: The drive and readout microwave signals of each qubit are combined and sent to the sample through a pair of transmission lines with total attenuation 70 dB and filtered at 4 K and 300 mK. A microwave circulator at 20 mK protects the chip from the amplifier noise. The signals are amplified by 36 dB at 4 K by two cryogenic HEMT amplifiers (CIT Cryo 1) with noise temperature 5 K. The reflected readout pulses are amplified and demodulated at room temperature. The IQ quadratures of the demodulated signals are sampled at 1 GS/s by a 4-channel data acquisition system (Acqiris DC282).

S4. Readout Errors

Errors in our readout scheme are discussed in detail in [13] for a single qubit. First, incorrect mapping $|0\rangle \rightarrow 1$ or$|1\rangle \rightarrow 0$ of the projected state of the qubit to the dynamical state of the resonator can occur, due to the stochastic nature of the switching between the two dynamical states. As shown in Fig. S4.1, the probability p to obtain the outcome 1 varies continuously from 0 to 1 over a certain range of drive power $P_{\rm d}$ applied to the readout. When the shift in power between the two $p_{|0\rangle,|1\rangle}(P_{\rm d})$ curves is not much larger than this range, the two curves overlap and errors are significant even at the optimal drive power where

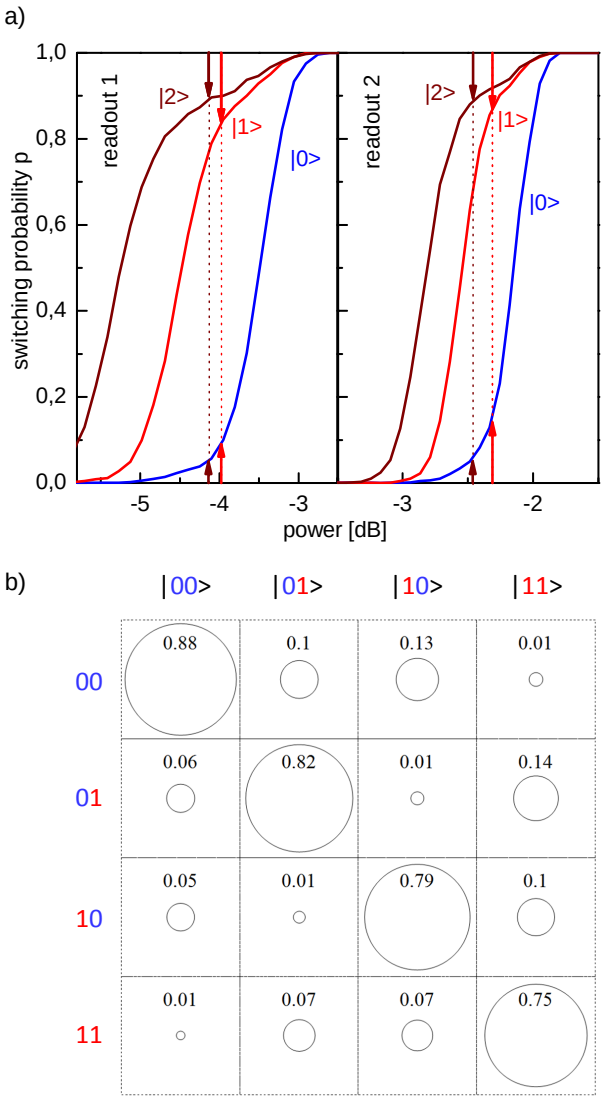

Figure 1:
(a) Switching probability p of each readout as a function of its peak driving power, when its qubit is prepared in state $|0\rangle$ (blue), $|1\rangle$ (red), or $|2\rangle$ (brown), with the other qubit being far detuned. The arrows indicate the readout errors where the contrast is optimal with (brown) and without (red) $|1\rangle \rightarrow |2\rangle$ shelving. (b) Readout matrix giving the probabilities of the four ab outcomes, for the four computational input states $|uv\rangle$, when using $|1\rangle \rightarrow |2\rangle$ shelving.

the difference in p is maximum. Second, even in the case of non overlapping $p_{|0\rangle,|1\rangle}(P_{\rm d})$ curves, the qubit initially projected in state$|1\rangle$ can relax down to $|0\rangle$ before the end of the measurement, yielding an outcome 0 instead of 1. The probability of these two types of errors vary in opposite directions as a function of the frequency detuning $\Delta = \nu_{\rm R} - \nu > 0$ between the resonator and the qubit, so that a compromise has to be found for Δ. As explained in the main text, we use a shelving method to the second excited state in order to improve the readout contrast $c = Max\left(p_{|1\rangle} - p_{|0\rangle}\right)$, with a microwave π pulse at frequency ν_{12} bringing state $|1\rangle$ into state $|2\rangle$ just before the readout pulse. The smallest errors $e_0^{\rm I,II}$ and $e_1^{\rm I,II}$ when reading $|0\rangle$ and $|1\rangle$ are found for $\Delta_{\rm I} = 440\,{\rm MHz}$ and $\Delta_{\rm II} = 575\,{\rm MHz}$: $e_0^{\rm I} = 5\%$ and $e_1^{\rm I} = 13\%$ (contrast $c_{\rm I} = 1 - e_0^{\rm I} - e_1^{\rm I} = 82\%$), and $e_0^{\rm II} = 5.5\%$ and $e_1^{\rm II} = 12\%$ ($c_{\rm II} = 82\%$). When using the $|1\rangle \rightarrow |2\rangle$ shelving before readout, $e_0^{\rm I} = 2.5\%$ and $e_2^{\rm I} = 9.5\%$ (contrast $c_{\rm I} == 1 - e_0^{\rm I} - e_2^{\rm I} = 88\%$), and $e_0^{\rm II} = 3\%$ and $e_2^{\rm II} = 8\%$ ($c_{\rm II} = 89\%$). These best results are very close to those obtained in [12], but cannot however be exploited for simultaneous readout of the two qubits.

Indeed, when the two qubits are measured simultaneously, we find an influence of the projected state of each qubit on the outcome of the readout of the other one. In order to to minimize this spurious effect, we increase the detuning $\Delta_{\rm I,II}$ up to $\sim 1\,{\rm GHz}$ with respect to previous optimal values. An immediate consequence shown in Fig. S4.1(a) is a reduction of the $c_{\rm I,II}$ contrasts. The errors when reading $|0\rangle$ and $|1\rangle$ are then $e_0^{\rm I} = 10\,\%$ and $e_1^{\rm I} = 16\,\%$ (contrast $c_{\rm I} = 74\%$) and $e_0^{\rm II} = 12\,\%$ and $e_1^{\rm II} = 15\,\%$ (contrast $c_{\rm II} = 73\%$). When shelving the qubit in state $|2\rangle$, the errors are $e_0^{\rm I} = 5\,\%$, $e_2^{\rm I} = 11\,\%$ (contrast $c_{\rm I} = 84\%$), $e_0^{\rm II} = 5\,\%$, $e_2^{\rm II} = 12\,\%$ (contrast $c_{\rm I} = 83\%$). The readout errors are captured in the 4×4 readout matrix $\mathcal{R}$ shown in Fig. S4.1(c), that gives the probabilities $p_{\rm uv}$ of the four possible outcomes for the different input states using the $|1\rangle \rightarrow |2\rangle$ shelving technique. This matrix $\mathcal{R}$ is used to correct the readout errors only when doing state tomography, and not when the running the algorithm once. The cause of the readout crosstalk in our processor is discussed in [11].

S5. Algorithm Fidelity

The fidelity of each possible outcome $ab \in \{00, 01, 10, 11\}$ of our algorithm is given as

$$f_{ab} = p_{ab/|ab\rangle} / \left(p_{ab/|00\rangle} + p_{ab/|01\rangle} + p_{ab/|10\rangle} + p_{ab/|11\rangle}\right),$$

where $p_{ab/|uv\rangle}$ is the conditional probability for obtaining ab when the state $|uv\rangle$ has been marked by the oracle O_{uv}. Table 1 shows these probabilities $p_{ab/|uv\rangle}$ for all possible combinations of ab and $|uv\rangle$ as well as the fidelities f_{ab}. The average fidelity of the algorithm is 59.1 %.

$ab/\|uv\rangle$	$\|00\rangle$	$\|01\rangle$	$\|10\rangle$	$\|11\rangle$	$\sum$	f_{ab}
00	0.666	0.192	0.188	0.122	1.168	57.0 %
01	0.127	0.554	0.071	0.122	0.874	63.4 %
10	0.128	0.106	0.615	0.239	1.088	56.5 %
11	0.079	0.148	0.126	0.517	0.870	59.4 %

Table 1: Conditional probabilities $p_{ab/|uv\rangle}$ and statistical fidelities f_{ab} for all possible outcomes ab, measured for our version of Grover's algorithm.

References

[1] F. R. Ong *et al.*, Phys. Rev. Lett. 106, 167002 (2011).